PHYSICAL REVIEW LETTERS

Numerical Study of Dynamo Action at Low Magnetic Prandtl Numbers

Y. Ponty,[1] P. D. Mininni,[2] D. C. Montgomery,[3] J.-F. Pinton,[4] H. Politano,[1] and A. Pouquet[2]

[1]*CNRS UMR6202, Laboratoire Cassiopée, Observatoire de la Côte d'Azur, BP 4229, Nice Cedex 04, France*
[2]*ASP/NCAR, P.O. Box 3000, Boulder, Colorado 80307-3000, USA*
[3]*Department of Physics and Astronomy, Dartmouth College, Hanover, New Hampshire 03755, USA*
[4]*CNRS UMR5672, Laboratoire de Physique, École Normale Supérieure de Lyon, 46 Allée d'Italie, 69007 Lyon, France*

We present a three-pronged numerical approach to the dynamo problem at low magnetic Prandtl numbers P_M. The difficulty of resolving a large range of scales is circumvented by combining direct numerical simulations, a Lagrangian-averaged model and large-eddy simulations. The flow is generated by the Taylor-Green forcing; it combines a well defined structure at large scales and turbulent fluctuations at small scales. Our main findings are (i) dynamos are observed from $P_M = 1$ down to $P_M = 10^{-2}$, (ii) the critical magnetic Reynolds number increases sharply with P_M^{-1} as turbulence sets in and then it saturates, and (iii) in the linear growth phase, unstable magnetic modes move to smaller scales as P_M is decreased. Then the dynamo grows at large scales and modifies the turbulent velocity fluctuations.

The generation of magnetic fields in celestial bodies occurs in media for which the viscosity ν and the magnetic diffusivity η are vastly different. For example, in the interstellar medium the magnetic Prandtl number $P_M = \nu/\eta$ has been estimated to be as large as 10^{14}, whereas in stars such as the Sun and for planets such as the Earth, it can be very low ($P_M < 10^{-5}$, the value for the Earth's iron core). Similarly in liquid breeder reactors and in laboratory experiments in liquid metals, $P_M \ll 1$. At the same time, the Reynolds number $R_V = UL/\nu$ (U is the rms velocity; L is the integral scale of the flow) is very large, and the flow is highly complex and turbulent, with prevailing nonlinear effects rendering the problem difficult to address. The dynamo instability is governed by the magnetohydrodynamics (MHD) equations,

$$\partial_t \mathbf{v} + \mathbf{v} \cdot \nabla \mathbf{v} = -\nabla \mathcal{P} + \mathbf{j} \times \mathbf{B} + \nu \nabla^2 \mathbf{v} + \mathbf{F}, \quad (1)$$

$$\partial_t \mathbf{B} + \mathbf{v} \cdot \nabla \mathbf{B} = \mathbf{B} \cdot \nabla \mathbf{v} + \eta \nabla^2 \mathbf{B}, \quad (2)$$

together with $\nabla \cdot \mathbf{v} = 0$, $\nabla \cdot \mathbf{B} = 0$, and assuming a constant mass density. Here, $\mathbf{v}$ is the velocity field, and $\mathbf{B}$ is the magnetic field. $\mathcal{P}$ is the pressure and $\mathbf{j} = \nabla \times \mathbf{B}$ is the current density. $\mathbf{F}$ is a forcing term, responsible for the generation of the flow (buoyancy and Coriolis in planets and mechanical drive in experiments).

Several mechanisms have been studied for dynamo action, both analytically and numerically, involving, in particular, the role of helicity [1] (i.e., the correlation between velocity and its curl, the vorticity) for dynamo growth at scales larger than that of the velocity, and the role of chaotic fields for small-scale growth of magnetic excitation (for a recent review, see [2]). If the stretching and folding of magnetic field lines by velocity gradients overcome dissipation, dynamo action takes place above a critical magnetic Reynolds number R_M^c, with $R_M = P_M R_V = UL/\eta$. Dynamo experiments based on constrained helical

flows of liquid sodium have been successful [3]. However, these experimental setups do not allow for a complete investigation of the dynamical regime, and many groups have searched to implement unconstrained dynamos [4]. Two difficulties arise: first, turbulence now becomes fully developed with velocity fluctuations reaching up to 40% of the mean; second, it is difficult to produce flows in which the helicity is more or less uniformly distributed spatially at the small scales, so that it is difficult to assess the effect of helical turbulent inverse cascades on the dynamo. Recent direct numerical simulations (DNS) address the case of randomly forced, nonhelical flows with magnetic Prandtl numbers from 1 to 0.1. The results obtained are not unambiguous: it is shown in [5] that dynamo action can be inhibited for $P_M < 1/4$, while it is observed in [2] that the dynamo threshold increases as $P_M^{-1/2}$ down to $P_M \sim 0.3$. Experiments made in von Kármán geometries (either spherical or cylindrical) have reached R_M values up to 60 [6]. Also, MHD turbulence at low P_M has been studied in the idealized context of turbulent closures [7]. In this context, turbulent dynamos are found, and the dependences of R_M^c upon three quantities are studied, namely, P_M, the relative rate of helicity injection, and the forcing scale. An increase of $\sim 20\%$ in R_M^c is observed as P_M decreases from 1 to $\sim 3 \times 10^{-5}$. Recently, the Kazantsev-Kraichnan [8] model of δ-correlated velocity fluctuations has been used to study the effect of turbulence. It has been shown that the threshold increases with the rugosity of the flow field [9].

There is therefore a strong motivation to study how the dynamo threshold varies as P_M is progressively decreased, for a given flow. In this Letter we focus on a situation where the flow forcing is not random but generates a well defined geometry at large scales, with turbulence developing naturally at small scales as the R_V increases. This situation complements recent investigations [2,5,9] and is quite relevant for planetary and laboratory flows.

Specifically, we consider the swirling flow resulting from the Taylor-Green (TG) forcing [10]:

$$\mathbf{F}_{\mathrm{TG}}(k_0) = 2F \begin{bmatrix} \sin(k_0 x)\cos(k_0 y)\cos(k_0 z) \\ -\cos(k_0 x)\sin(k_0 y)\cos(k_0 z) \\ 0 \end{bmatrix}. \quad (3)$$

This force generates flow cells that have locally differential rotation and helicity, two key ingredients for dynamo action [1,2]. In our numerical resolutions, we have chosen not to impose on the flow field the symmetries of the Taylor-Green forcing [11] and to set $k_0 = 2$ so that dynamo action is free to develop at scales larger or smaller than the forcing scale $k_f = k_0\sqrt{3}$. The flow generated by the TG force has motivated several numerical studies in the regime $P_M \sim 1$ [11,12]; it also shares similarities, particularly at large Reynolds numbers, with the Maryland, Cadarache, and Wisconsin sodium experiments [4]. Its global integrated helicity is zero over the whole domain. However local fluctuations of helicity are always present in the flow—here, we mean that the probability density function of kinetic helicity is centered about zero but has wings (growing with R_V); but even in one TG cell the net helicity (integrated over space) is zero.

Our numerical study begins with DNS in a 3D periodic domain. The code uses a pseudospectral algorithm, an explicit second order Runge-Kutta advance in time, and a classical dealiasing rule—the last resolved wave number is $k = N/3$ where N is the number of grid points per dimension. Resolutions from 64^3 to 512^3 grid points are used, to cover P_M from 1 to 1/5. However, DNS are limited in the Reynolds numbers and the (lowest) P_M they can reach. We then use a second method, the LAMHD (or α) model, in which we integrate the Lagrangian-averaged MHD equations [13,14]. This formulation leads to a drastic reduction in the degrees of freedom at small scales by the introduction of smoothing lengths α_V and α_M. The fields are written as the sum of filtered (smoothed) and fluctuating components: $\mathbf{v} = \mathbf{u_s} + \delta\mathbf{v}$, $\mathbf{B} = \mathbf{B_s} + \delta\mathbf{B}$, with $\mathbf{u_s} = G_{\alpha_V} \otimes \mathbf{v}$, $\mathbf{B_s} = G_{\alpha_M} \otimes \mathbf{B}$, where "$\otimes$" stands for convolution and G_α is the smoothing kernel at scale α, $G_\alpha(\mathbf{r}, t) = \exp[-r/\alpha]/4\pi\alpha^2 r$. Inversely, the rough fields can be written in terms of their filtered counterparts as $\mathbf{v} = (1 - \alpha_V^2\nabla^2)\,\mathbf{u_s}$ and $\mathbf{B} = (1 - \alpha_M^2\nabla^2)\,\mathbf{B_s}$. In the resulting equations, the velocity and magnetic field are smoothed, but not the fields' sources, i.e., the vorticity and the current density [15]. This model has been checked in the fluid case against experiments and DNS of the Navier-Stokes equations [16], as well as in MHD [14]. Finally, in order to reach still lower P_M, we implement a large-eddy simulation (LES) model. LESs are commonly used and well tested in fluid dynamics against laboratory experiments and DNS in a variety of flow configurations [17], but their extension to MHD is still in its infancy (see, however, [18]). We use a scheme as introduced in [19], aimed at integrating the primitive MHD equations with a turbulent

velocity field all the way down to the magnetic diffusion with no modeling in the induction equation but with the help of a dynamical eddy viscosity [20]:

$$\nu(k, t) = 0.27[1 + 3.58(k/K_c)^8]\sqrt{E_V(K_c, t)/K_c}; \quad (4)$$

K_c is the cutoff wave number of the velocity field, and $E_V(k, t)$ is the one-dimensional kinetic energy spectrum. A consistency condition for our approach is that the magnetic field fluctuations be fully resolved when $2\pi/K_c$ is smaller than the magnetic diffusive scale $\ell_\eta \sim L/R_M^{3/4}$.

The numerical methods, parameters of the runs, and associated characteristic quantities are given in Table I. In all cases, we first perform a hydrodynamic run, lasting about 10 turnover times, to obtain a statistically steady flow. Then we add a seed magnetic field and monitor the growth of the magnetic energy E_M for a time that depends on the run resolution; it is of the order of 1 magnetic diffusion time $\tau_\eta = (2\pi)^2/\eta$ at 64^3, but it drops down to $\tau_\eta/5$ at 512^3. We define the magnetic energy growth rate as $\sigma = d\log E_M/dt$, computed in the linear regime (t is in units of large scale turnover time). The dynamo threshold corresponds to $\sigma = 0$. For each configuration (Table I), we make several MHD simulations with different P_M, varying η, and for a fixed R_V defined by the hydrodynamic run. We

TABLE I. Run parameters: code used, linear grid resolution N, Reynolds number R_V, integral length scale L (defined as $L = 2\pi \int k^{-1}E_V(k)dk/\int E_V(k)dk$), critical magnetic Reynolds number R_M^c, inverse magnetic Prandtl number $1/P_M^c$, wave number k_{max} with the largest magnetic energy density, characteristic wave number k_D of magnetic field gradients (defined as the maximum of the current density spectrum), and kinetic spectral index ρ in the range $[k_{max}, k_D]$ (computed as a linear estimate). The values of ρ, L, and U used in the definitions of the Reynolds and magnetic Prandtl numbers are computed as time averages during the steady state of the hydrodynamic simulation; k_{max} and k_D are computed as time averages during the linear regime of the dynamo simulation closest to R_M^c.

| code	N	R_V	L	R_M^c	$1/P_M^c$	k_{max}	k_D	ρ
DNS	64	30.5	2.15	28.8	1.06	2	5	$\cdots$
DNS	64	40.5	2.02	31.7	1.28	2	5	$\cdots$
DNS	64	128	1.9	62.5	2.05	4	9	$\cdots$
DNS	128	275	1.63	107.9	2.55	5	11	-2.15
DNS	256	675	1.35	226.4	2.98	7	21	$\sim -5/3$
DNS	512	874.3	1.31	192.6	4.54	9	26	$\sim -5/3$
LAMHD	64	280	1.68	117.3	2.38	6	11	$\cdots$
LAMHD	128	678.3	1.35	256.6	2.64	8	12	$\sim -5/3$
LAMHD	128	880.6	1.32	242.1	3.64	9	22	$\sim -5/3$
LAMHD	256	1301.1	1.3	249.3	5.22	9	31	$\sim -5/3$
LAMHD	512	3052.3	1.22	276.4	11.05	10	45	$\sim -5/3$
LES	128	2236.3	1.37	151.9	14.72	5	21	$-5/3$
LES	256	5439.2	1.39	141	38.57	5	31	$-5/3$
LES	512	13395	1.34	144.4	96.92	5	45	$-5/3$
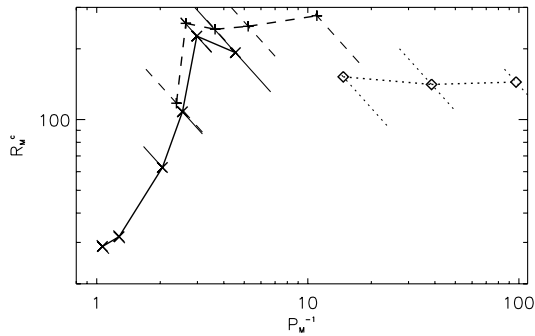
FIG. 1. R_M^c for dynamo action versus inverse P_M. Symbols are $\times$ (DNS), $+$ (LAMHD), and $\diamond$ (LES). Transverse lines indicate error bars in the determination of R_M^c, as the distance between growing and decaying runs at a constant R_V.
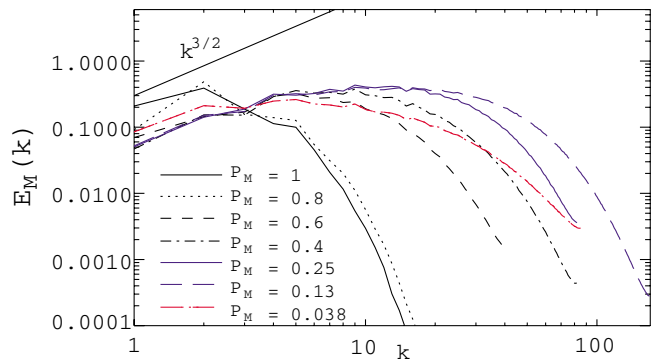

FIG. 2 (color). Magnetic spectra for $P_M = 1$ to $P_M = 0.4$ (DNS), $P_M = 0.25, 0.13$ (LAMHD), $P_M = 0.038$ (LES), at a time within the linear growth of magnetic energy; ($P_M = 1$, $R_V = 30.5$), ($P_M = 0.8$, $R_V = 40.5$), ($P_M = 0.6$, $R_V = 275$), ($P_M = 0.4$, $R_V = 675$), ($P_M = 0.25$, $R_V = 1301$), ($P_M = 0.13$, $R_V = 3052$), ($P_M = 0.038$, $R_V = 5439$); magnetic Reynolds number set 10% above threshold.

bound the marginal growth between clearly decaying and growing evolutions of the magnetic energy.

At $P_M = 1$, the dynamo self-generates at $R_M^c = 30$. As P_M is lowered, we observe in the DNS that the threshold reaches $R_M^c = 70$ at $P_M = 0.5$ and then increases steeply to $R_M^c = 226$ at $P_M = 0.3$; at lower P_M it does not increase anymore, but drops slightly to a value of 200 at $P_M = 0.2$ (Fig. 1 and Table I). We then continue with LAMHD simulations to reach lower P_M. To ensure the consistency of the method, we have run overlapping DNS and LAMHD simulations in the range $P_M = 0.4$–0.2. We have reached a good matching of the growth or decay rates [for identical (P_M, R_M) parameters] when using filtering scales related by $\alpha_V/\alpha_M = P_M^{3/4}$ (note that it preserves the dimensional relationship between magnetic and kinetic dissipation scales [14]). Our observation with the LAMHD computations is that the steep increase in R_M^c to a value over 250 is being followed by a plateau for P_M values down to 0.09. We do note a small but systematic trend of the LAMHD simulations to overestimate the threshold compared to DNS. We attribute it to the increased turbulent intermittency generated by the α model, but further investigations are required to describe fully this effect. As turbulence becomes fully developed, LES modeling becomes justified [17,19] and allows us to further our investigation; with this model we observe that the threshold for dynamo self-generation remains constant, of the order of $R_M^c \sim 150$, for P_M between 10^{-1} and 10^{-2}.

In regards to the generation of dynamo action in the Taylor-Green geometry we thus find (i) at all P_M investigated a dynamo threshold exists, (ii) as P_M drops below 0.2–0.3, the critical R_M^c levels and remains of the order of 200, and (iii) the steep initial increase in R_M^c is identified with the development of an inertial range in the spectra of kinetic energy; as the kinetic energy spectrum grows progressively into a Kolmogorov $k^{-5/3}$ spectrum, R_M^c ceases to have significant changes—cf. Table I.

We plot in Fig. 2 the magnetic energy spectra $E_M(k)$ during the linear growth phase, at identical instants when

normalized by the growth rate. Four features are noteworthy: first, the dynamo grows from a broad range of modes; second, the maximum of $E_M(k)$ moves progressively to smaller scales as P_M decreases, a result already found numerically in [2]; third, a self-similar magnetic spectrum, $E_M(k) \sim k^{3/2}$, develops at the beginning during the linear growth phase—in a similar fashion as to Kazantsev [8] and as found in other numerical simulations of dynamo generation by turbulent fluctuations [2,5]. This feature persists when the flow has a well defined mean geometry in addition to turbulence. Last, we observe that the initial magnetic growth at small scales is always followed by a second phase where the magnetic field grows in the (large) scales of the Taylor-Green flow. Figure 3 shows renderings of the magnetic energy and compare low and high Reynolds number cases. When the dynamo is generated at low Reynolds number ($R_V \sim 30$ and $P_M = 1$), the magnetic field is smooth. As P_M decreases and the dynamo grows from a turbulent field, one first observes a complex magnetic field pattern—for $t < 40$, in the example shown in Fig. 3 (center). But as nonlinear effects develop (here for
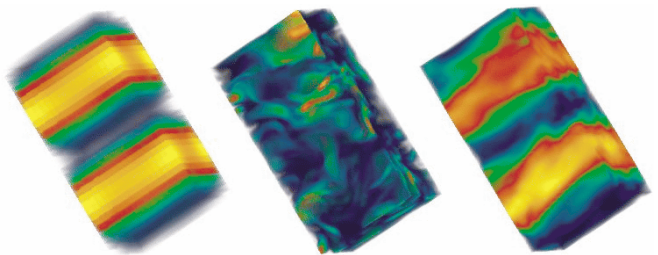

FIG. 3 (color). Spatial distributions of the magnetic energy for two Taylor-Green cells (DNS): $P_M = 1$, $R_V \sim 30$ at $t = 20$ (left), $P_M = 0.4$, $R_V = 675$ at $t = 20$ (center), and $t = 150$ (right).
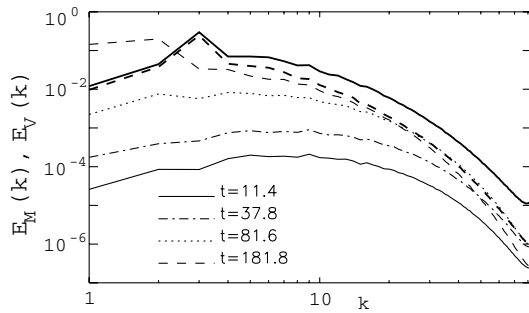
FIG. 4. Magnetic (thin line) and kinetic (thick line) spectra as a function of time at $P_M = 0.4$ (DNS).

times $t > 40$) a large scale mode ($k = 2$) dominates the growth with a structure that is similar to the one at low R_V. The initial growth of small-scale magnetic fields and the subsequent transfer to a large scale dynamo mode is also clearly visible on the development in time of the magnetic and kinetic energies, in a high R_V case, as shown in Fig. 4. During the linear growth, modes increase in a self-similar fashion, accounting for the complexity of the dynamo field—cf. Fig. 3 (center). At a later time, the large scale field grows and the kinetic energy spectrum $E_V(k)$ is progressively modified at inertial scales. The spectral slope changes from a scaling close to Kolmogorov $k^{-5/3}$ to a steeper decrease, compatible with the k^{-3} law observed experimentally [21]. The effect is to modify the turbulent scales and to favor the dynamo mode that is allowed by the large scale flow geometry. This is consistent with the experimental observation of a k^{-5} magnetic spectrum in the Karlsruhe dynamo experiment [22]. It also corroborates the claim [23] that the saturation of the turbulent dynamo starts with the backreaction of the Lorentz force on the turbulent fluctuations; the mean flow is altered at a later stage as shown in [14] where we describe the complete saturation stage.

To conclude, we have implemented a combination of DNS, LAMHD modeling, and LES. We show that for the Taylor-Green flow forcing there is a strong increase in the critical magnetic Reynolds number for dynamo action when P_M is decreased, directly linked to the development of turbulence; it is followed by a plateau on a large range of P_M from ~ 0.25 to $\sim 10^{-2}$. Thus, in a situation with both a mean flow and turbulent fluctuations, we find that the selection of the dynamo mode results from a subtle interaction between the large and small scales. Further discussions of the numerical procedure and results will be reported elsewhere [14].

[1] H. K. Moffatt, *Magnetic Field Generation in Electrically Conducting Fluids* (Cambridge University Press, Cambridge, 1978).

[2] N. E. L. Haugen, A. Brandenburg, and W. Dobler, Phys. Rev. E **70**, 016308 (2004); A. Brandenburg and K. Subramanian, Phys. Rep. (to be published).

[3] A. Gailitis, Magnetohydrodynamics **1**, 63 (1996); A. Tilgner, Phys. Rev. A **226**, 75 (1997); R. Steglitz and U. Müller, Phys. Fluids **13**, 561 (2001); A. Gailitis *et al.*, Phys. Rev. Lett. **84**, 4365 (2000).

[4] See the special issue on MHD dynamo experiments [Magnetohydrodynamics **38** (2002)].

[5] A. Schekochihin *et al.*, New J. Phys. **4**, 84 (2002); A. Schekochihin *et al.*, Phys. Rev. Lett. **92**, 054502 (2004).

[6] N. L. Peffley, A. B. Cawthrone, and D. P. Lathrop, Phys. Rev. E **61**, 5287 (2000); M. Bourgoin *et al.*, Phys. Fluids **14**, 3046 (2002).

[7] R. H. Kraichnan and S. Nagarajan, Phys. Fluids **10**, 859 (1967); J. Léorat, A. Pouquet, and U. Frisch, J. Fluid Mech. **104**, 419 (1981).

[8] A. P. Kazantsev, Sov. Phys. JETP **26**, 1031 (1968); R. H. Kraichnan, Phys. Fluids **11**, 945 (1968).

[9] I. Rogachevskii and N. Kleeorin, Phys. Rev. E **56**, 417 (1997); S. Boldyrev and F. Cattaneo, Phys. Rev. Lett. **92**, 144501 (2004); D. Vincenzi, J. Stat. Phys. **106**, 1073 (2002).

[10] M. Brachet, C. R. Acad. Sci. Paris Ser. IV **311**, 775 (1990).

[11] N. L. Dudley and R. W. James, Proc. R. Soc. London A **425**, 407 (1989); C. Nore *et al.*, Phys. Plasmas **4**, 1 (1997).

[12] L. Marié *et al.*, Eur. Phys. J. B **33**, 469 (2003); M. Bourgoin *et al.*, Phys. Fluids **16**, 2529 (2004).

[13] D. D. Holm, Physica (Amsterdam) **170D**, 253 (2002).

[14] P. D. Minnini, D. C. Montgomery, and A. Pouquet, Phys. Fluids **17**, 035112 (2005); Phys. Rev. E (to be published); P. D. Mininni *et al.*, astro-ph/0412071 [Astrophys. J. (to be published)].

[15] D. C. Montgomery and A. Pouquet, Phys. Fluids **14**, 3365 (2002).

[16] S. Y. Chen *et al.*, Phys. Fluids **11**, 2343 (1999); S. Y. Chen *et al.*, Physica (Amsterdam) **133D**, 66 (1999).

[17] C. Meneveau and J. Katz, Annu. Rev. Fluid Mech. **32**, 1 (2000).

[18] A. Pouquet, J. Léorat, and U. Frisch, J. Fluid Mech. **77**, 321 (1976); A. Yoshizawa, Phys. Fluids **30**, 1089 (1987); M. Theobald, P. Fox, and S. Sofia, Phys. Plasmas **1**, 3016 (1994); W.-C. Müller and D. Carati, Phys. Plasmas **9**, 824 (2002); B. Knaepen and P. Moin, Phys. Fluids **16**, 1255 (2004).

[19] Y. Ponty, H. Politano, and J. F. Pinton, Phys. Rev. Lett. **92**, 144503 (2004).

[20] J. P. Chollet and M. Lesieur, J. Atmos. Sci. **38**, 2747 (1981).

[21] A. Alemany *et al.*, J. Mec. **18**, 277 (1979).

[22] U. Müller, R. Stieglitz, and S. Horanyi, J. Fluid Mech. **498**, 31 (2004).

[23] F. Pétrélis and S. Fauve, Eur. Phys. J. B **22**, 273 (2001).